Numerical insights on the seismic behavior of a non-isolated historical masonry tower

(Article begins on next page)

31 October 2024

NUMERICAL INSIGHTS ON THE SEISMIC BEHAVIOR OF A NON-ISOLATED HISTORICAL MASONRY TOWER

Giovanni Castellazzi[1], D'Altri Antonio Maria[1*], Stefano de Miranda[1], Andrea Chiozzi[2], Antonio Tralli[2]

[1] DICAM, Dept. of Civil, Chemical, Environmental and Materials Engineering, University of Bologna, Viale del Risorgimento 2, 40136 Bologna, Italy
[2] Engineering Department, University of Ferrara, Via Saragat 1, 44122 Ferrara, Italy

*corresponding author: antoniomaria.daltri2@unibo.it

ABSTRACT

In this paper, numerical insights on the seismic behavior of a non-isolated historical masonry tower are presented and discussed. The tower under study is the main tower of the fortress of San Felice sul Panaro, a town located near the city of Modena (Italy). Such a tower is surrounded by adjacent structural elements and, therefore, is not isolated. This historical monument has been hit by the devastating seismic sequence occurred in May 2012 in the Northern part of the Emilia region (the so-called "Emilia Earthquake"), showing a huge and widespread damage. Here, in order to understand the behavior of the structure, its interaction with the adjacent buildings and the reasons of the occurred damage, advanced numerical analyses (both nonlinear static and dynamic) are performed on a 3D finite element model with different levels of constraint supplied by the adjacent structural elements and a detailed comparison between the simulated damage and the actual one is carried out. The results of the conducted numerical campaign show a good agreement with the actual crack pattern, particularly for the model of the tower that considers the adjacent structural elements.

Keywords: Non-isolated tower; Masonry; Seismic damage; FE nonlinear analysis, Cultural Heritage; 2012 Emilia Earthquake

1   Introduction

Masonry towers represent a considerable part of the existing architectural heritage in Italy, as well as in many other European countries. Unfortunately, these structures, which are noticeable for their prevalent high-rise peculiarity, present a huge seismic vulnerability. The seismic behavior of these structures depends on specific features such as the slenderness of the structure, the presence on the top part of vulnerable and heavy elements (bell cells, merlons, bells, etc.) and also on the presence of adjacent shorter structural elements. Indeed, several towers and belfries are placed in contact with adjacent lower structures, e.g. belfries alongside the church or towers connected to the curtain wall. As reported in the Italian guidelines on cultural heritage (DPCM 9/2/2011), the presence of horizontal constraints at different heights of a tower may deeply change its structural behavior. On one hand, they can restrict the actual slenderness (thus reducing the period). On the other hand, they can induce local stiffening which may produce stress state concentrations and, therefore, severe localized damages. Moreover, they typically act as mono-lateral constrains (depending on the masonry toothing between the parts) which might possibly produce pounding.

The numerical assessment of the structural behavior of historical masonry towers is still a challenging task for contemporary engineers. Since the study of this kind of structures is characterized by significant difficulties related to the description of the complex nonlinear behavior of the masonry, as well as of complex geometries and boundary conditions, in most cases the Finite Element Method (FEM) has been used in order to face these issues. In particular, the macro-modeling approach in which the masonry is typically modeled as an equivalent homogeneous continuum is the most suitable as compared with other approaches, such as micro-modeling, due to its lower computational effort.

Since the first attempts of fully 3D FE modeling of historical towers in the nineties, see for instance Macchi et al. (1993) and Casolo (1998), the numerical techniques for the analysis of these structures have been considerably developed. In order to implement the strong nonlinearities of masonry, advanced nonlinear

analyses have been performed on several masonry towers considering complex nonlinear constitutive laws. For instance, in Carpinteri et al. (2005), aiming at assessing the behavior of a historic tower in the case of increase in the tilt mechanism, the results of a nonlinear analysis have been presented. In Preciado (2015), the seismic vulnerability assessment of different types of towers and slender masonry structures (e.g. light houses and minarets) has been performed. In Pineda (2016), static, modal and transient analyses have been performed on a medieval tower model, aiming at obtaining the role of the materials in the structural damage and the effect of the strengthening materials on the increase of structural safety. Relevant is the study reported in Peña et al. (2010), where the seismic assessment of an old masonry tower has been addressed by developing three FE models with different levels of complexity, whereas a comparative numerical study on a 12th-century masonry tower has been described in Milani et al (2012). To assess the safety of the tower under seismic loads, the authors employed different numerical analyses such as nonlinear static, limit, and fully nonlinear dynamic analyses. In Casolo et al. (2013), ten existing masonry towers located in the Po Valley (Italy) have been analyzed in the presence of seismic excitations. The seismic vulnerability assessment of eight historical masonry towers, located in the North-Eastern region of Italy, has been carried out in Valente and Milani (2016a) by means of simplified approaches based on nonlinear static pushover analyses, whereas in Valente and Milani (2016b) nonlinear dynamic analyses have been performed on the same 3D FE models of the towers using a real accelerogram. In Acito et al. (2014), the results of a wide numerical campaign conducted on the clock tower in Finale Emilia (Italy), collapsed during the main shock of the devastating Emilia earthquake seismic sequence (2012), have been collected, while, in Tiberti et al. (2016), a numerical insight on the historical masonry Castle of Finale Emilia has been presented. In Sarhosis et al. (2017) a simple predictive approach for the seismic vulnerability of existing masonry towers has been proposed, whereas in Valente and Milani (2017) the effects of geometrical features on the seismic response of masonry towers have been investigated.

Notwithstanding this quite huge amount of literature, the numerical assessment of the structural interaction between a tower and its adjacent lower buildings still presents difficulties that make an already complex problem even more complicated. Indeed, in the aforementioned cases, for the sake of simplicity, the towers have been studied as isolated towers, even if in several cases they were linked to shorter buildings.

Conversely, in Bartoli et al. (2006) and Bartoli et al. (2013) the evaluation of the seismic reliability of a masonry tower has been performed by using a dynamic characterization of an elastic FEM, where the in situ dynamic tests results permitted to estimate the restraint degree offered by the neighbor building. Moreover, in D'Ambrisi et al. (2012), the aim of the performed structural identification was the evaluation of the Young's modulus of the masonry and of the constraint effect given by the adjacent constructions to a historical masonry tower. In Pieraccini et al. (2014), the numerical model of the Mangia's tower in Siena (Italy) was identified according to the results of the experimental investigation performed by means of an interferometric radar: the effects of the neighboring buildings at the lower level were modeled as linear springs. The aforementioned dynamic identifications have been performed in the elastic field, which is a strong limitation when studying the behavior of masonry structures. Finally, in Bartoli et al. (2016), one of the masonry towers of San Gimignano (Italy) was investigated, and several FE nonlinear analyses were performed to evaluate its seismic risk. The effects of the presence of adjacent constructions at the lower level of the tower were assessed by analyzing two limit cases: isolated tower and confined tower (with different levels of constraint). As a result, strong differences between isolated and confined tower FE nonlinear static results were obtained, in terms of both capacity curves and damage pattern. However, since the analyzed tower did not present seismic damage, no experimental findings were available to validate the actual seismic behavior of the tower.

In this paper, the attention is focused on the main tower (the keep) of the fortress of San Felice sul Panaro (Fig. 1), a town located near the city of Modena (Italy). Such a tower is linked to adjacent structural elements and, therefore, is not isolated. The fortress has been hit by the Emilia Earthquake and presented a huge and widespread damage.

Aiming at the refurbishment of the whole fortress, a multi-disciplinary project promoted by the Municipality of San Felice sul Panaro and involving five Italian universities (Bologna, Ferrara, Genoa, Modena & Reggio

Emilia and Parma) is going on. In this project, starting from the analysis of the geometrical and constructive features of the Emilian historical fortresses, the interpretation of their seismic vulnerability has been presented in Cattari et al. (2014), based on an accurate damage assessment after the earthquake of May the 20th and 29th, 2012. Moreover, advanced mesh generation approaches that semi-automatically transform 3D point clouds into 3D FE models have been recently proposed and applied to the San Felice sul Panaro fortress in Castellazzi et al. (2015), Castellazzi et al. (2017), Castellazzi et al. (2016b) and Bitelli et al. (2016). Finally, experimental in situ tests have been extensively performed on the fortress (Mazzotti et al. 2016) and few preliminary findings on the seismic behavior of the main tower of the fortress have been reported in Castellazzi et al. (2016a).

Within this framework, here we present and discuss numerical insights on the seismic behavior of the main tower of the fortress. In particular, in order to understand the behavior of the structure, its interaction with the adjacent buildings and the reasons of the occurred damage, advanced numerical analyses, both nonlinear static and dynamic, have been performed on a 3D FE model of the tower considering several levels of constraint offered by the adjacent structural elements. Numerical results of the conducted numerical campaign show a reasonable agreement with the actual crack pattern, particularly for the model of the tower that considers the adjacent portions.

The paper is organized as follows. Section 2 presents the description of the tower under study. Section 3 describes the numerical analyses performed (natural frequencies analyses, nonlinear static analyses, nonlinear dynamic analyses). Section 4 shows the numerical modeling of the tower, both in terms of FE discretization and constitutive model for masonry. Section 5 collects the results of the performed analyses while Section 6 presents a comparison of the obtained results with the actual crack pattern. Concluding remarks end the paper (Section 7).

2 Description of the tower under study

The tower under study is the main tower (South-East tower) of the San Felice sul Panaro Fortress (Fig. 1a). Such a tower is connected to the South Entrance building along its West side (see Fig. 1b); while in its North front it is joined with the curtain wall. Both of these adjacent parts are lower than half of the height of the tower.
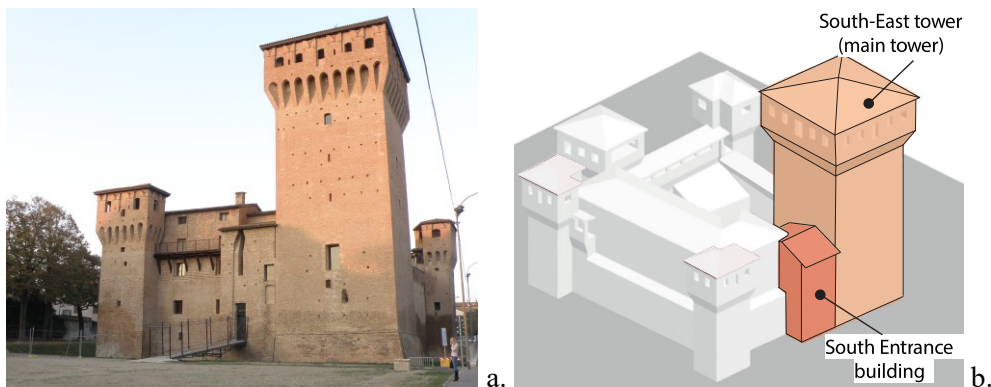

Fig. 1 - San Felice sul Panaro fortress and its constitutive elements.

The main tower of San Felice sul Panaro fortress is 32 m high with an almost square plant with sides of slightly more than 10 m. As evidenced by Fig. 2, the tower is composed of seven layers of different kinds: three groined vaults and three timber decks as well as a timber-trussed roof. The thickness of the tower's walls ranges from 2.5 m at the bottom up to 0.4 m at the top. Several openings of different sizes are irregularly placed along the tower. The tower is characterized by the presence of an upper part (the crowning) which presents a larger plan, realized through masonry corbels, which allows enlarging the perimeter overhanging from the wall below. The external walls of the tower crowning are constituted by merlons connected by little arches (see South front and East front in Fig. 2). Moreover, a series of eight walls perpendicular to the perimeter sides are present in the tower crowning and sustain the complex roof structure (see E-W section and S-N section in Fig. 2).
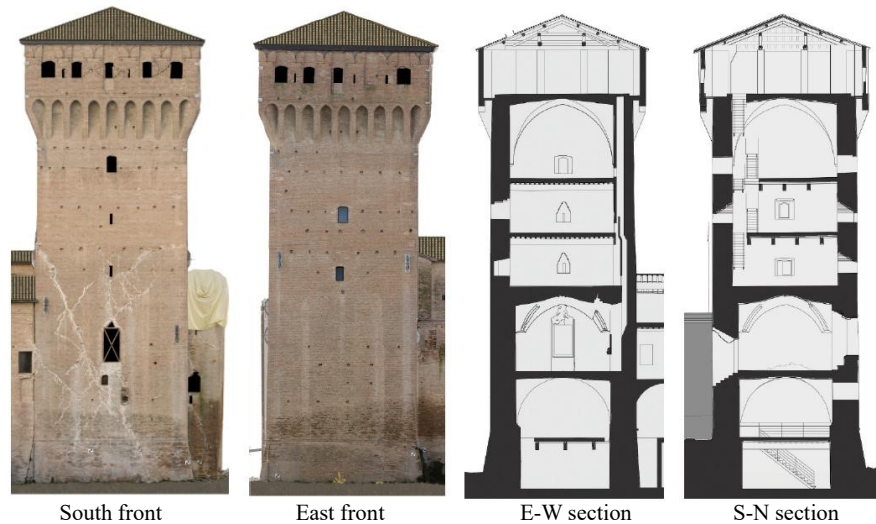
4

| South front | East front | E-W section | S-N section |

Fig. 2 - The main tower of the San Felice sul Panaro fortress.

2.1   Emilia earthquake damage

The Emilian territory has experienced a heavily damaging seismic sequence during the second half of May 2012, whose biggest shocks occurred within the provinces of Modena and Ferrara. An accurate description of the seismic sequence and its effects on Emilian medieval fortress is reported in Cattari et al. (2014). The main shocks have been recorded on May the 20th (M_w=5.9) and May the 29th (M_w=5.8) (Dolce et al. 2012a and 2012b). The epicenters of these shocks have been located at about 10 and 5 km from San Felice sul Panaro, respectively (see Fig. 3).
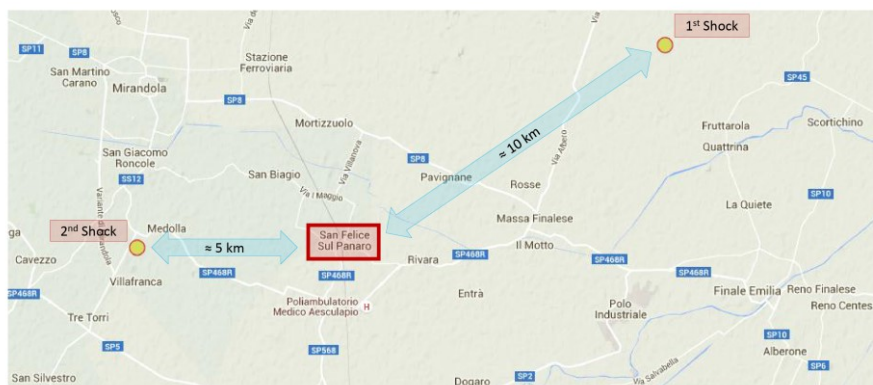

Fig. 3 - Main shocks of the Emilia earthquake (May 20th and 29th, 2012).

As a result, the fortress presented an extensive damage (Fig. 4) in terms of both the collapse of the crowning of the minor towers (Fig. 4a) and the appearance of several cracks of different seriousness on the main tower wall, particularly in the South and North side (Fig. 4b and Fig. 4c, respectively). The most relevant cracks of the main tower consist in diagonal cracks, clearly visible in the lower half of the South (Fig. 4b) and North (Fig. 4c) front. These cracks start from the half height of the tower's trunk (from the side of the South entrance building, Fig. 1b) and end at the ground level of the opposite side of the tower, see Fig. 4b and Fig. Fig. 4c. By inspecting Fig. 4b, it appears that no relevant cracks are placed in the top part of the main tower's trunk. This is probably due to the presence of steel tie-rods in this portion of the tower, added in the 90s, which may have limited the cracks opening. However, the results of an accurate thermo-graphic campaign, reported in Mazzotti et al. (2016), reveal that such part of the structure presents several minor cracks.

Fig. 4 - San Felice sul Panaro fortress after the Emilia Earthquake (2012): (a) collapse of the minor towers' crowning, main tower's South front (b) and North front (c).

3   Performed analyses

One of the main purposes of the paper consists in assessing the effect, on the seismic behavior of the tower, of the interaction between the tower itself and the other parts of the fortress. In order to reach such a purpose while keeping low the computational cost and maintaining simple the model, the tower has been modeled together with some portions of its adjacent elements (highlighted in red in Fig. 5). Then, to account for the presence of the non-modeled parts of the fortress (which are deformable), supports on the section surfaces (yellow surfaces in Fig. 5a) have been implemented and the stiffness of the considered adjacent parts (red portions in Fig. 5) has been reduced by decreasing their Young's modulus E_{adj}. In particular, E_{adj} is assumed equal to E_m/δ, where E_m is the masonry Young's modulus and δ is a coefficient ($\delta \geq 1$). Several scenarios corresponding to different values of δ have been analyzed. Of course, when $\delta \to \infty$ the Young's modulus of the adjacent parts $E_{adj} \to 0$, which corresponds to the case of isolated tower. In order to overcome possible numerical drawbacks, this condition has been implemented by totally removing the red parts of Fig. 5a.
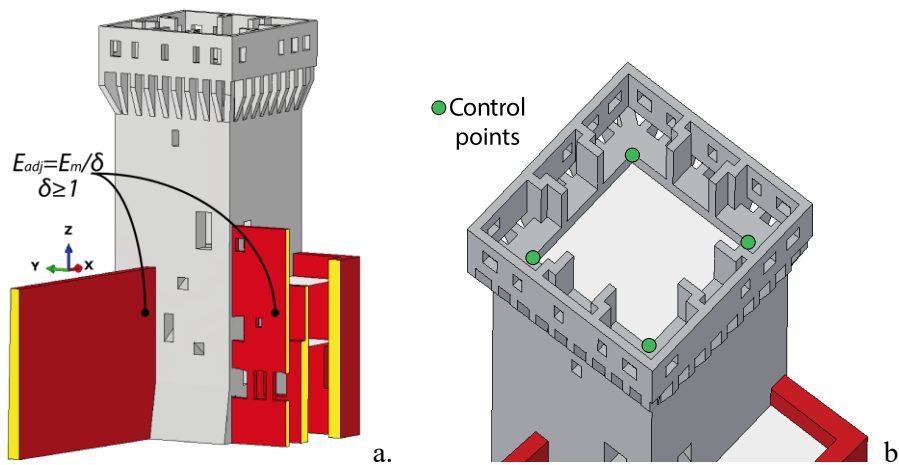

Fig. 5 - 3D FE model of the case study: adjacent parts (a) and control points (b).

Different types of analyses have been performed. In particular, natural frequencies analyses, nonlinear static (pushover) analyses and nonlinear dynamic analyses have been carried out. In the last two analysis types, the displacement of the tower's top has been computed as the average of the displacements of the four evenly-spaced control points depicted in Fig. 5b, as suggested in Lagomarsino et al. (2015).

Pushover analysis is a nonlinear static procedure generally used to determine the structural behavior against horizontal forces. Basically, the numerical model of the structure is loaded with a proper distribution of horizontal static forces, which are gradually increased aiming at pushing the structure out from the linear field. Here, fully 3D pushover analyses have been performed on a 3D model, using horizontal forces proportional to

the modal shapes computed in natural frequencies analyses. These analyses are carried out until a drop of the 20% of the base shear, which conventionally represents the collapse condition of the structure.

Nonlinear dynamic analyses have been carried out accounting for the real accelerogram to which the tower has been subjected. As anticipated, the tower has been subjected to two big shocks (May 20th and 29th). Indeed, a sequence, close in space and time, of strong shocks of similar intensity can induce damage cumulation in the masonry structure, which represents a very challenging issue recently investigated by Casolo (Casolo, 2017). For the tower under study, after the first shock, the main tower already presented some cracks of which, unfortunately, only a very poor documentation is available. Complete collapses were observed after the second shock. Furthermore, the only accelerogram available in the proximity of the fortress is the one recorded on May 29th, 2012 at the *SAN0* station (which was installed in San Felice sul Panaro only after the May 20th (Dolce et al. 2012a and 2012b)) located at approximately 150 meters from the fortress, see Fig. 6. Such accelerogram is characterized by a Peak Ground Acceleration (PGA) equal to $0.220g$, $0.175g$ and $0.312g$ in NS, EW and vertical directions, respectively (see Fig. 7 (Luzi et al. 2008)). According to the above considerations, in the performed nonlinear dynamic analyses we exclusively considered the seismic action recorded during the second shock assuming an initially uncracked structure. Although Italian guidelines on cultural heritage (DPCM 9/2/2011) recommend to conduct nonlinear dynamic analyses considering at least three different accelerograms normalized to the expected spectral acceleration in order to perform the vulnerability assessment of a historical structure, the authors were interested in comparing the simulated damage with the one experienced by the tower. Therefore, dynamic simulations have been carried out with the aforementioned recorded earthquake only.

Fig. 6 - Location of the *SAN0* station with respect to the fortress.

25-seconds nonlinear dynamic simulations (see Fig. 7) have been performed considering several load cases. For the sake of brevity, three cases are reported: (i) EW component only, (ii) NS and EW components, (iii) NS, EW and vertical components of the earthquake recorded on May 29th. In particular, the measured accelerogram has been applied to the nodes at the base of the tower for the horizontal components only, whereas the vertical component has been conceived as a gravitational load (which varies over time), defined as the algebraic sum, at each time instant, of g plus the amplitude of the vertical component of the accelerogram. In such analyses, the aforementioned constraint condition on the yellow surfaces of Fig. 5a has been considered through the implementation of kinematic master-slave constrains between a node at the base of the tower (master) and the nodes on the yellow surfaces of Fig. 5a (slaves). The geometric nonlinearity was accounted for both in pushover and nonlinear dynamic analyses, aiming at considering the possible reduction of the structure's capacity due to displacements outside the permitted range of pertinence of the linearity hypothesis.
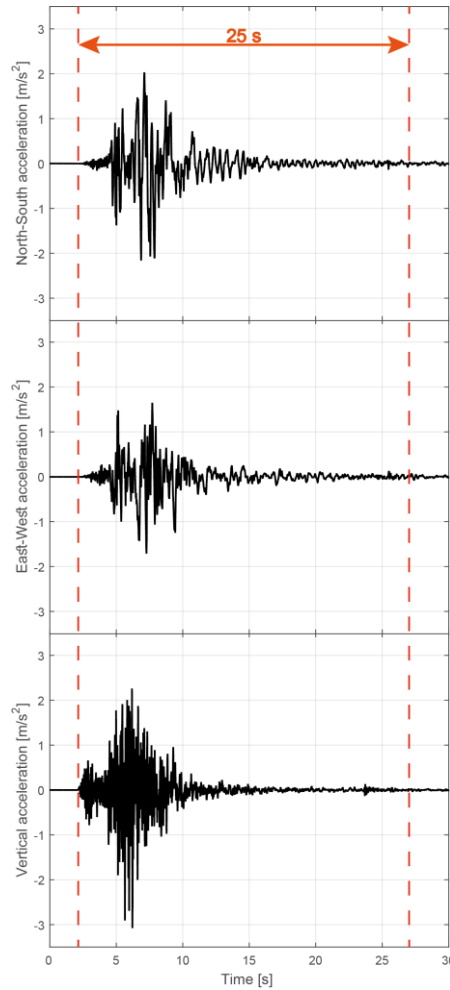
Fig. 7 - Accelerograms recorded the May 29th, 2012 at the *SAN0* station (Fig. 6).

4   Numerical modeling

In this section, the FE discretization of the case study as well as the adopted constitutive law for masonry are described.

4.1   *Finite element discretization*

Numerical computations have been carried out by means of fully 3D FE meshes (tetrahedron elements) with different level of refinement (see Fig. 8). Such meshes have been obtained starting from a CAD-based geometric modeling developed thanks to a detailed survey. The meshes are designed to capture the global structural behavior of the tower: also, the coarse mesh depicted in Fig. 8 appears appealing having at least three tetrahedron elements on the thickness of the tower trunk's walls (see the magnified portion). The horizontal axes of the model (X and Y) substantially correspond to the cardinal directions (SN and EW, respectively).
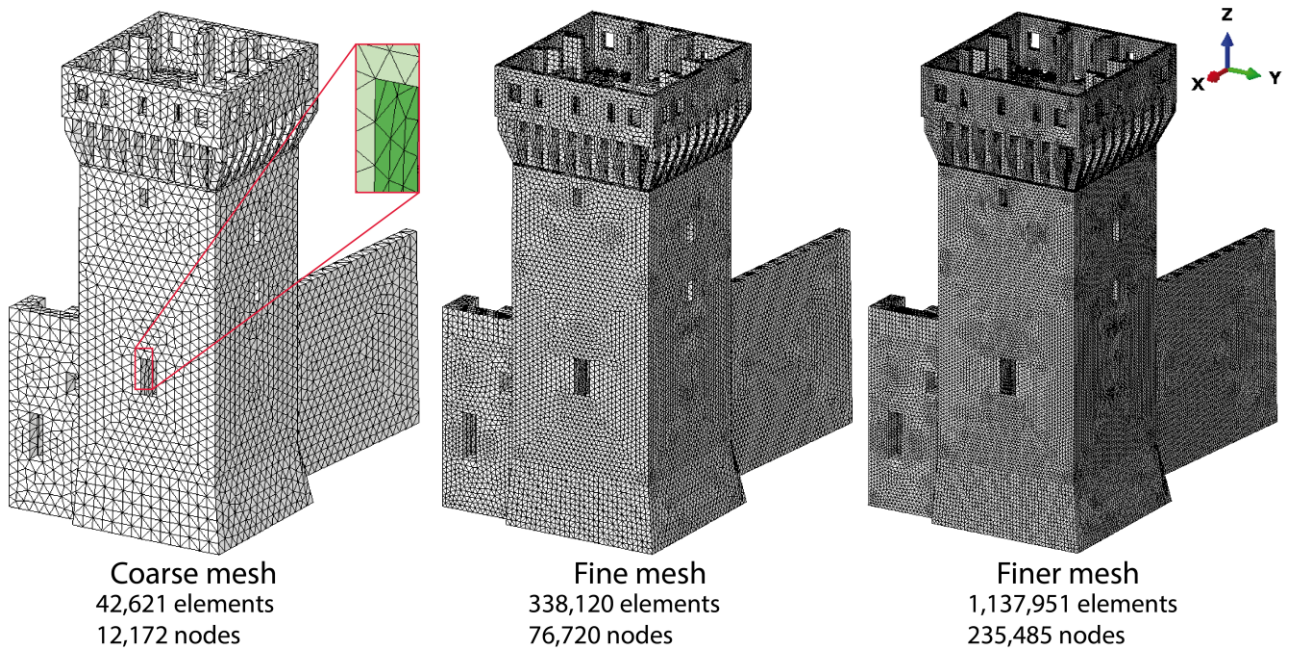
Fig. 7 - Adopted meshes.

Modeling floors and vaults has always been a very relevant issue when dealing with numerical models (D'Altri et al. 2017). In order to limit the computational effort and meshing drawbacks, masonry vaults and timber floors have been modeled through equivalent plates (i.e. with the same in-plane stiffness). Such a simplification, commonly accepted in the literature (Cattari et al. 2012), is motivated by the fact that we aim at assessing the global structural behavior of the tower.

4.2 Constitutive law for masonry

The definition of suitable constitutive laws for masonry is still an open problem. Masonry is a composite material characterized by an overall orthotropic behavior, both in the elastic and inelastic fields (Page 1981). However, the macro-modeling approach finds some difficulties in the description of the orthotropic behavior in linear as well as nonlinear fields. Even though interesting advances have been achieved in continuum damage models for masonry materials (Luciano and Sacco 1997, Milani et al. 2007, Mistler et al. 2007) their applicability to 3D large-scale structures is still controversial due to several factors such as their limitation to 2D problems and the difficulty in setting the many mechanical parameters. Therefore, it is commonly accepted in the literature the utilization of isotropic models for masonry after an adaptation of the parameters to fit an average behavior between vertical and horizontal compression.

In this paper, isotropic material behavior both in the elastic and inelastic fields was supposed. Such an assumption appears specifically appealing for the particular structure under study. Indeed, the presence of very thick walls makes the use of complex orthotropic constitutive laws as questionable as the use of more robust isotropic models. Here, the isotropic constitutive model utilized to perform pushover and nonlinear dynamic analyses is the so called Concrete Damage Plasticity (CDP) model (Fig. 9), which is available within the Abaqus software (2014). Although it has been conceived for concrete, the CDP model has been often successfully used for masonry, see for instance (Castellazzi et al. 2017, Tiberti et al. 2016, Acito et al. 2014). Its features as well as the adopted parameters are briefly described in the following. The interested reader is referred to Abaqus (2014) and Castellazzi et al. (2017) for further details.

The simulation of the mechanical behavior of materials with different strength in tension and in compression is contemplated in the CDP model and distinct damage variables in tension and compression are implemented, see Fig. 9a and Fig. 9b. The mono-axial tensile and compression stresses σ_t and σ_c are computed through the following standard relationships:

$$\sigma_t = (1 - d_t)E_m\left(\varepsilon_t - \varepsilon_t^{pl}\right)$$

9

$$\sigma_c = (1 - d_c)E_m\left(\varepsilon_c - \varepsilon_c^{pl}\right)$$

where E_m is the undamaged elastic modulus, d_t and d_c are the damage variables in tension and in compression, ε_t and ε_c are the total strain in tension and in compression, ε_t^{pl} and ε_c^{pl} are the equivalent plastic strain in tension and in compression. Under cyclic loading conditions, the CDP model also takes into account the effect of closing of previously formed cracks, which results in the recovery of the compressive stiffness.
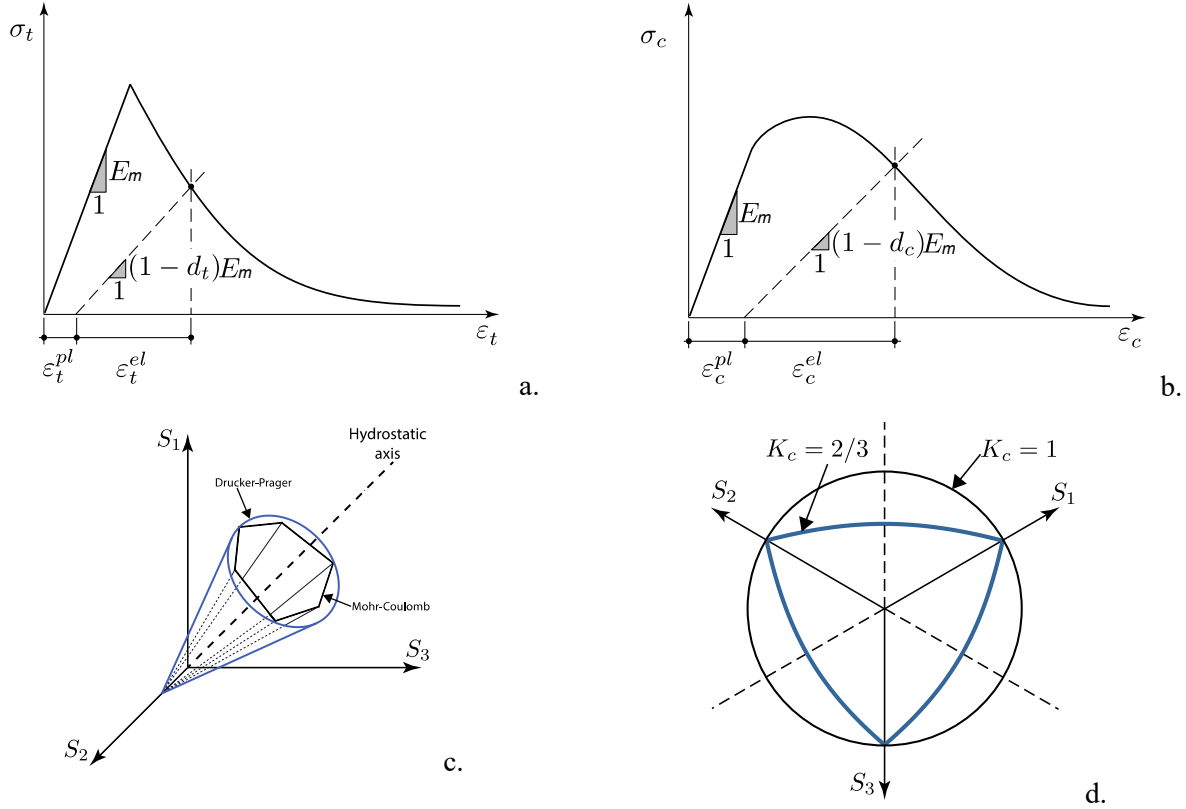

Fig. 9 - Concrete damage plasticity model: tensile (a) and compression (b) mono-axial inelastic curves, yield surfaces in the Westergaard space (c) and in the deviatoric plane (d).

A Drucker-Prager strength domain is assumed, altered by a K_c parameter (Figs. 9c-9d) which represents the ratio between the distance from the hydrostatic axis of the maximum compression and tensile stress, respectively. As advised in Abaqus (2014), the value 2/3 has been assumed for K_c. Moreover, the value 10° has been adopted as the dilatation angle of masonry and the ratio between the bi-axial, f_{b0}, and mono-axial, f_{c0}, compression strength has been assumed equal to 1.16 (Page 1981). In order to guarantee the global convergence of the algorithm in the nonlinear range, a smoothing of the tension corner has been implemented through an eccentricity parameter equal to 0.1 and 0.002 has been assumed as viscosity parameter. Indeed, as shown in Tiberti et al. 2016 and Castellazzi et al. 2017 through a sensitivity analysis, the overestimation of the collapse base shear when using this value of the viscosity parameter is substantially negligible for this kind of structures.

This constitutive model uses a fracture energy-based regularization to describe the softening in tension and compression (i.e. both tensile and compressive fracture energies are scaled in relation to the finite element size). In this way, the mesh size does not significantly influence the model response.

Since in-situ tests performed on the structure, which are available in Mazzotti et al. 2016, present inhomogeneous findings, reference to *Table C8A.2.1* of Circolare 617-02/02/2009 (DM 14/01/2008) is made in order to select the mechanical parameters of the material. Such parameters are chosen by considering the lowest knowledge level (the so-called *LC1* in Circolare 617-02/02/2009 (DM 14/01/2008) and a masonry typology with quite regular courses constituted by clay bricks and very poor mortar. The parameters used in

10

numerical analyses are collected in Table 1 and the adopted mono-axial inelastic stress-strain relationships for masonry are reported in Fig. 10. Such inelastic curves are reasonably comparable with those used in Tiberti et al. (2016) and Acito et al. (2016), where the numerical analyses of coeval and very similar masonry towers, which are located no more than 12 km far from the tower under study, have been presented. Indeed, medieval masonry materials in the region hit by the 2012 earthquakes seem to exhibit a quite similar and low strength (Borri et al. 2013). As it is still unknown how the tie-rods are connected to masonry walls, they have not been explicitly modelled and the same mechanical properties throughout the model for all masonry material have been adopted. In this paper, a masonry tensile strength value (f_t) equal to 0.12 MPa has been considered. In any case, a sensitivity analysis of the model response (in terms of pushover curve) to the tensile strength value is reported in the following. Finally, a linear variation of both compressive (d_c) and tensile (d_t) scalar damage variables from zero (for deformations which correspond to the stress peak, see Fig. 10) to 0.9 (for deformations which correspond to the lowest extremities of the softening branches, see Fig. 10) has been assumed.

Table 1 - Material properties used in the numerical analyses.

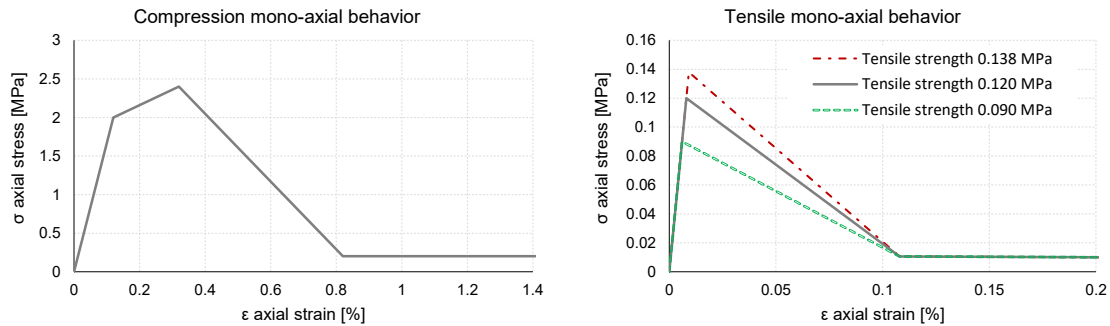| Material properties	Values
Young's modulus E_m [MPa]	1500
Poisson's ratio	0.2
Dilatation angle	10
Eccentricity	0.1
f_{b0}/f_{c0}	1.16
K_c	2/3
Viscosity parameter	0.002

Fig. 10 - Compression and tensile mono-axial inelastic curves.

5   Numerical results

In this section, the results of the performed analyses are discussed. Natural frequencies, nonlinear static and nonlinear dynamic analyses results are presented.

5.1   Natural frequencies analyses

First, aiming at assessing the accuracy of the FE models based on the meshes introduced Section 4.1 (Fig. 8), a natural frequencies comparison has been carried out, see Table 2. In particular, the isolated tower case ($\delta \rightarrow \infty$) has been analyzed. As can be noted in Table 2, the frequencies percentage differences between the coarse mesh and the finer one are extremely low, under the 3.5% for the first five modes. Therefore, the model based on the coarse mesh appears satisfying for natural frequencies analysis purposes and has been used in the following.

Table 2 - Natural frequencies comparison between the meshes depicted in Fig. 8.

Mode #	Finer fr. [Hz]	Fine fr. [Hz]	Var.%	Coarse fr. [Hz]	Var. %
1	1.865	1.872	0.36	1.892	1.37
2	1.896	1.903	0.37	1.923	1.39
3	4.271	4.303	0.73	4.388	2.66
4	6.658	6.726	1.01	6.895	3.48
5	6.693	6.756	0.93	6.914	3.18

In order to achieve a first preliminary assessment of the adjacent portions effects on the dynamic behavior of the tower, natural frequencies analyses have been conducted considering different configurations of the adjacent parts. In particular, six values of the adjacent parts Young's modulus have been considered, varying from the isolated tower ($\delta \to \infty$) to the non-isolated tower with $\delta = 1$. Natural frequencies and percentage variations with respect to the isolated tower case are collected in Table 3, whereas modal shapes of the extreme cases ($\delta \to \infty$ and $\delta = 1$) plus an intermediate case ($\delta = 10$) are illustrated in Fig. 11.

Table 3 - Natural frequencies.

Modes		Adjacent parts configuration					
#	Description	$\delta \to \infty$	$\delta = 100$	$\delta = 10$	$\delta = 5$	$\delta = 2$	$\delta = 1$
1	1st bend. EW fr.[Hz]	1.892	1.970	2.175	2.306	2.552	2.770
	Var.		4.1%	14.9%	21.9%	34.8%	46.4%
2	1st bend. NS fr.[Hz]	1.923	1.941	1.956	2.012	2.131	2.313
	Var.		0.9%	1.7%	4.6%	10.8%	20.3%
3	Torsional fr.[Hz]	4.388	4.686	4.712	4.750	4.773	4.954
	Var.		6.8%	7.6%	8.2%	8.8%	12.9%
4	2nd bend. EW fr.[Hz]	6.895	6.948	7.532	7.728	8.251	8.546
	Var.		0.8%	9.2%	12.1%	19.7%	23.9%
5	2nd bend. NS fr.[Hz]	6.914	6.930	6.985	7.007	7.092	7.319
	Var.		0.2%	1.0%	1.3%	2.5%	5.8%

As it can be noted from Table 3, the variation of the natural frequencies from the less rigid to the stiffest case is significant. In particular, such variation is more significant for the EW directed modal shapes (up to 46.4%) than the NS directed ones (up to 20.3%). Clearly, this is due to the greater stiffness of the constraint in the EW direction (South entrance building) respect to the one in the NS direction (curtain wall).
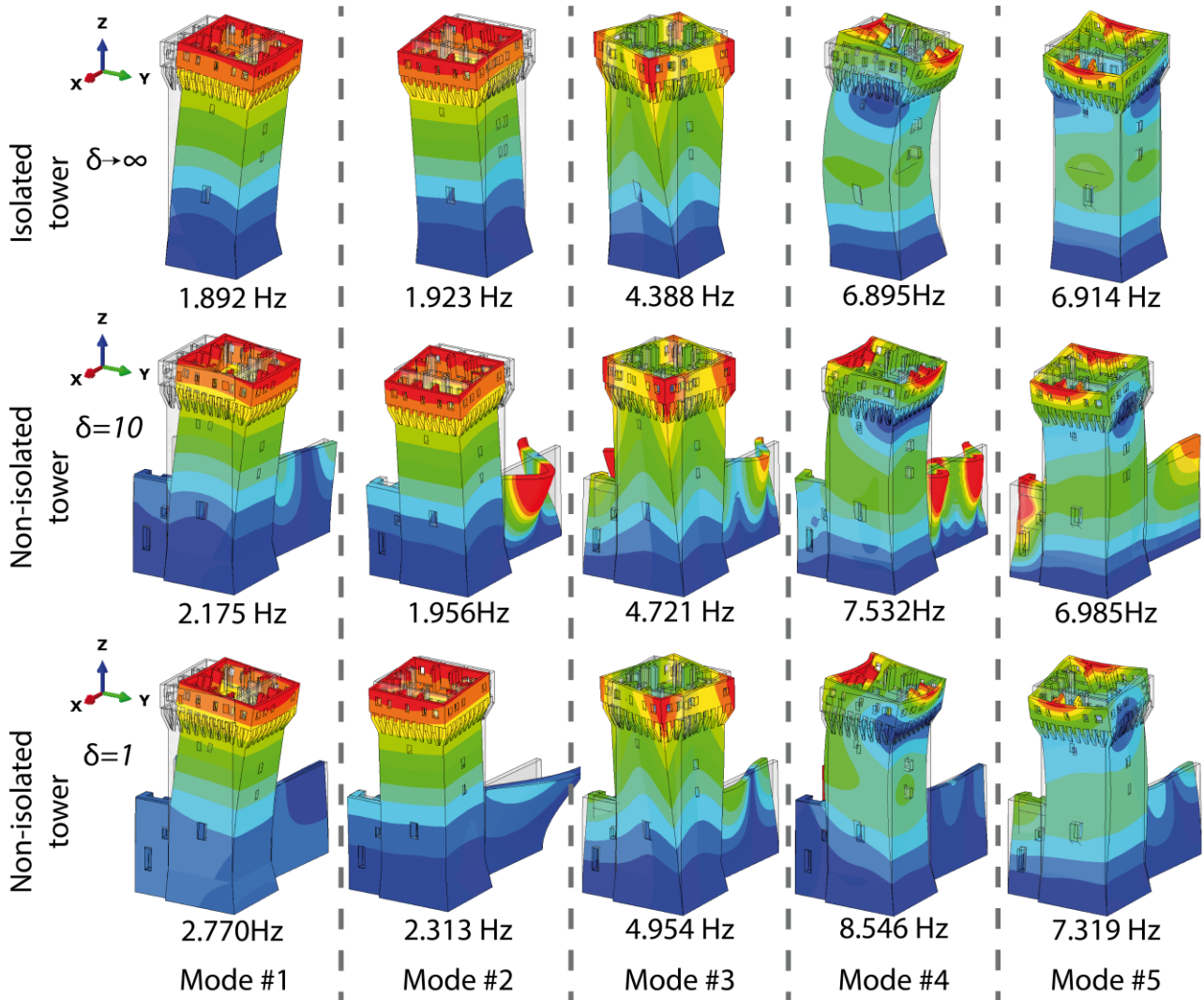
Fig. 11 - Modal shapes.

5.2 Nonlinear static analyses

In this section, the results of nonlinear static analyses are reported. As a preliminary step, in order to assess the mesh dependency of nonlinear analysis results, a comparison in terms of pushover curves (Fig. 12) and damage contour plots (Fig. 13) between the coarse and the fine mesh outcomes has been carried out for the isolated tower case ($\delta \to \infty$). As can be observed in Fig. 12, the pushover curves obtained using the two meshes are substantially equivalent. In addition, by inspecting Fig. 13 it emerges a very good agreement also in terms of damage pattern. According to these results and aiming at keeping the model as simple as possible, the FE model based on the coarse mesh has been used in the following nonlinear analyses.
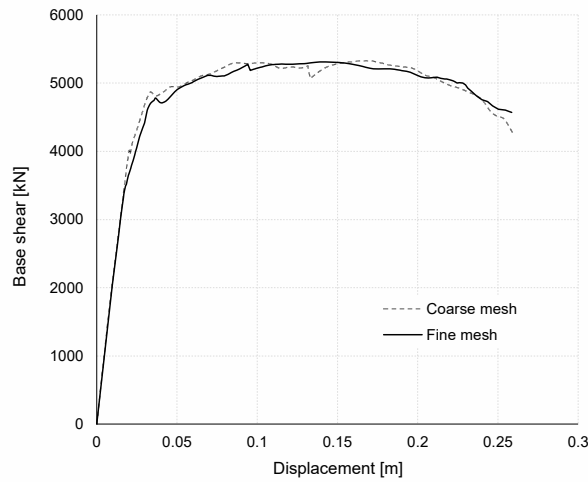
13

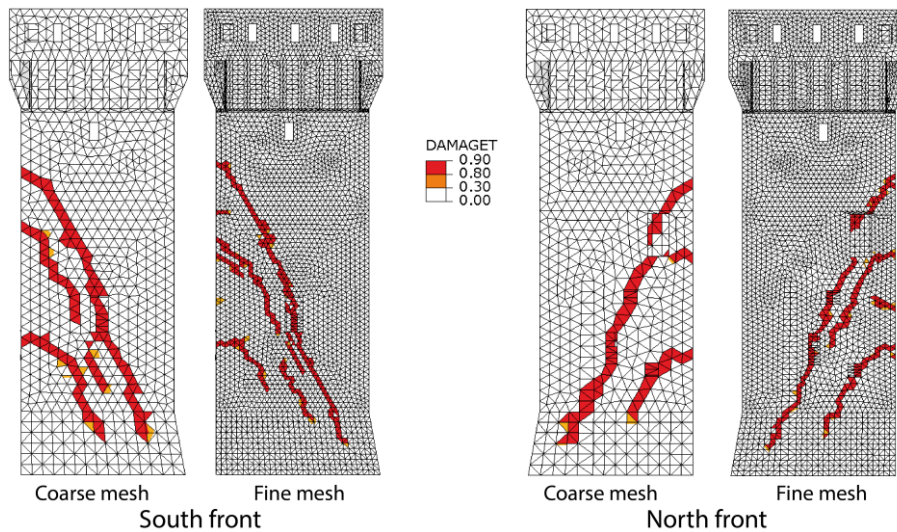Fig. 12 - Mesh influence on the pushover curve.

Fig. 13 - Mesh influence on the cracks distribution.

Beyond the choice of the mesh, in nonlinear analyses the constitutive model of the material plays a crucial role. As anticipated, the CDP model has been adopted in this paper (Abaqus 2014). Anyway, in order to further validate the consistency of the model response for the case under study, several nonlinear static analyses on the same mesh have been also performed using Diana (2013), adopting the crack model implemented within the software package (assuming mechanical parameters equivalent to the ones utilized in the CDP model, as carried out in Castellazzi et al. 2016a. A good agreement between the results obtained from the use of the two constitutive models has been observed. As an example, Fig. 14 depicts the comparison of the damage pattern obtained using the present CDP model and the one implemented in Diana for the East load case of the non-isolated tower. As can be noted, the simulated crack patterns are in good agreement.
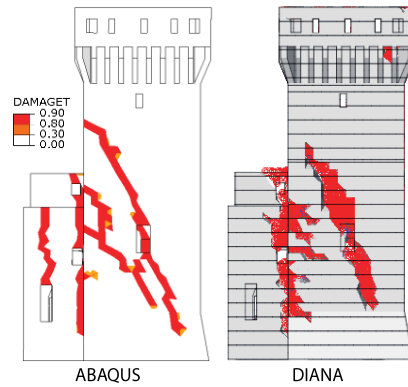
Fig. 14 - Example of damage contour plots comparison between Abaqus and Diana.

Finally, as already mentioned, a sensitivity analysis of the global response in terms of pushover curve to the tensile strength value f_t has been carried out. Particularly, pushover curves obtained by using the tensile strength values $f_t = 0.09 MPa$ and $f_t = 0.138\ MPa$, corresponding to the extreme values of cohesion $\tau_0 = 0.06\ MPa$ and $\tau_0 = 0.092\ MPa$ of *Table C8A.2.1* Circolare 617-02/02/2009 (following the simplified relationship $f_t = 1.5\tau_0$ (DM 14/01/2008)), have been compared with the one obtained using the value assumed in this paper $f_t = 0.12\ MPa$). The corresponding tensile mono-axial inelastic curves are depicted in Fig. 10. Fig. 15 collects the obtained pushover curves (West load case). As can be observed, a greater gap appears between the inelastic branches of the curves with 0.12 and 0.09 MPa rather than with 0.12 and 0.138 MPa. However, such discrepancy seems to be enclosed within the engineering accuracy tolerance and the pushover curves appear substantially equivalent. Therefore, in absence of reliable experimental results the tensile strength value equal to 0.12 MPa is, in the authors' opinion, a reasonable compromise for the case study at hand.
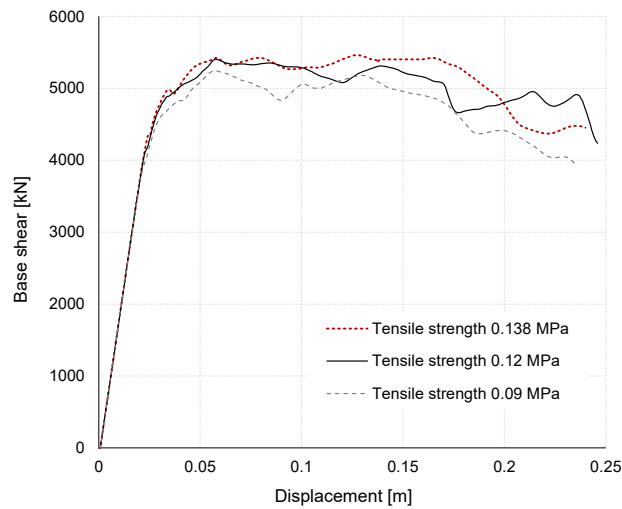

Fig. 15 - Tensile strength influence on the pushover curve.

In order to better highlight the differences between considering an isolated tower rather than a non-isolated tower and to not burden the text, nonlinear static analyses have been carried out on the extreme cases of isolated tower ($\delta \rightarrow \infty$) and non-isolated tower with $\delta = 1$ only. Fig. 16 shows the eight pushover capacity curves for each principal direction (East, West, South, North) of both the extreme cases. Of course, the reaction of the constraints in the yellow surfaces of Fig. 5 has been accounted for the computation of the base shear in the non-isolated tower case.
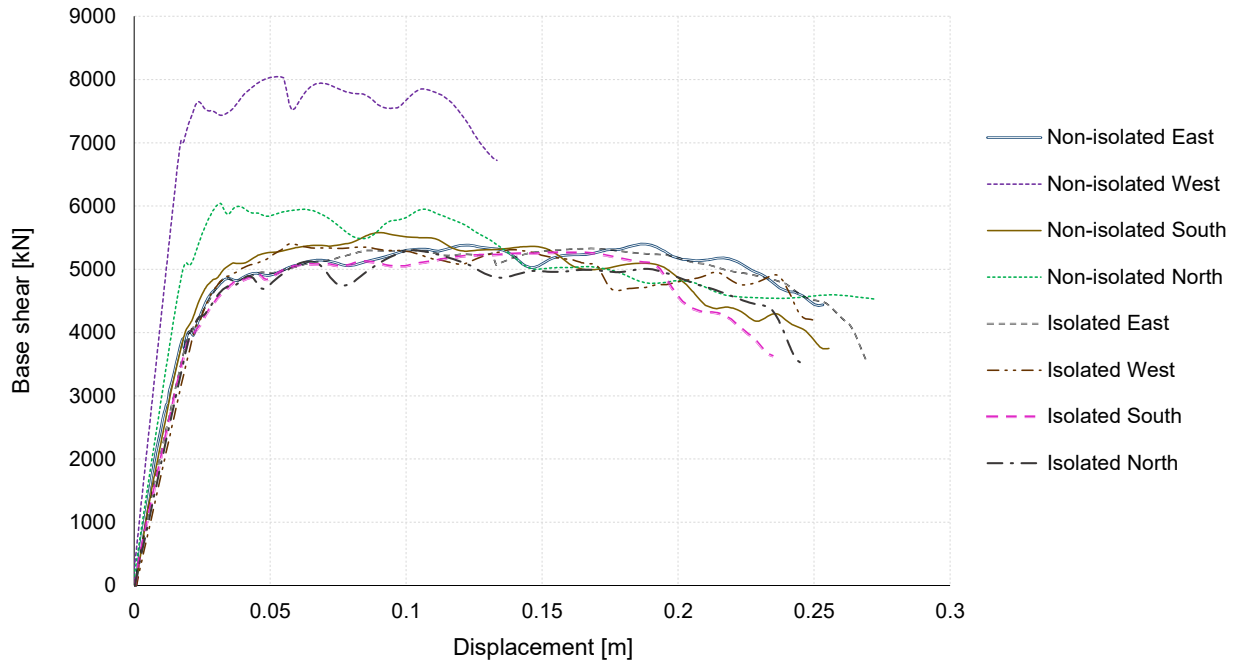
Fig. 16 - Pushover curves.

On one hand, pushover curves of the isolated tower are quite similar in each direction, exception made for the West case which presents a slightly upper curve.

On the other hand, non-isolated tower pushover curves are clearly sensible to adjacent parts. Indeed, stiffer elastic branches as well as curves with greater base shear values than the isolated tower can be observed. Furthermore, they considerably differ the one from the other depending on the direction of the applied horizontal force. In particular, pushover curves in the West and North directions show a considerable increment of the elastic branches slope and of the base shear, whereas such phenomena are less significant in the East and South directions. As could be expected, the adjacent parts have a significant role in the behavior of the tower particularly when the tower is pushed against them, i.e. when the adjacent parts present a horizontal compressive stress state.

Figs. 17-20 show the damage contour plots comparison between isolated and non-isolated tower provided by the pushover analyses for East, West, North and South directions of the horizontal force, respectively. For the sake of brevity, in such figures only the sides parallel to the direction of the horizontal forces are reported since they show the most significant damage. Such plots are taken in the displacement demand d_{dem} condition, evaluated as briefly reported in the Appendix (for quantitative values refer to Fig. 26). This condition conventionally represents the operation point of the tower for the considered design seismic action. It can be noted that, for all the cases of isolated tower, the main damage mechanism is represented by large diagonal cracks that extend for almost the whole height of the tower's trunk.

On one hand, the East directed force damage contour plots (Fig. 17) show that the damage pattern is slightly influenced by the adjacent parts. Indeed, in the elements between the tower and the adjacent parts the damage immediately appears for the presence of tensile stress peaks. This is in agreement with the little variation of the curves between the isolated and non-isolated tower, see Fig. 16 (East load case). Furthermore, no substantial damage pattern changes between the isolated and the non-isolated tower case are recorded for the North (Fig. 19) and South (Fig. 20) load cases.

On the other hand, concerning the results of a West directed force analysis (Fig. 18), the damage pattern is strongly affected by the presence of the adjacent buildings. In this case, indeed, the effect of the constraint offered by the South entrance building consists in confining the cracks to the upper parts of the tower's trunk, over the height of the adjacent parts.
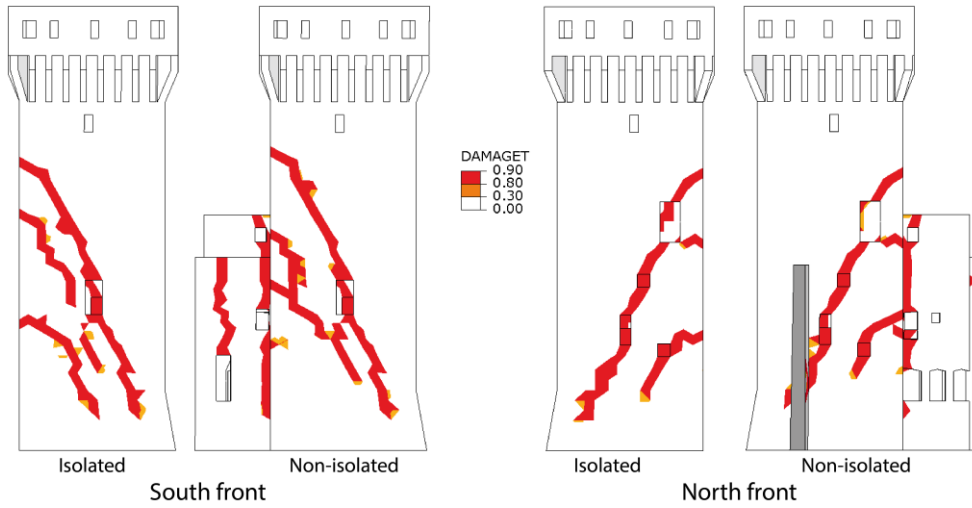
16

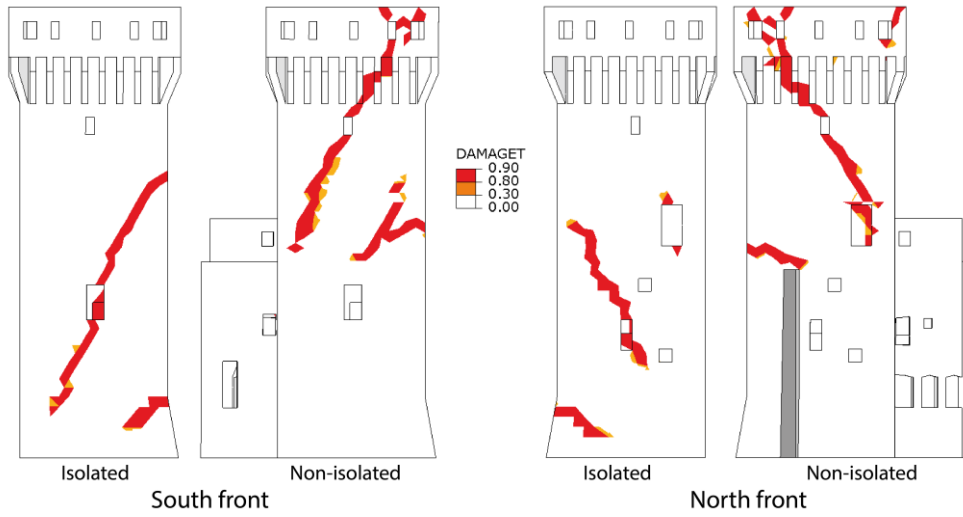Fig. 17 - Damage contour plots: East directed force (pushover analysis).

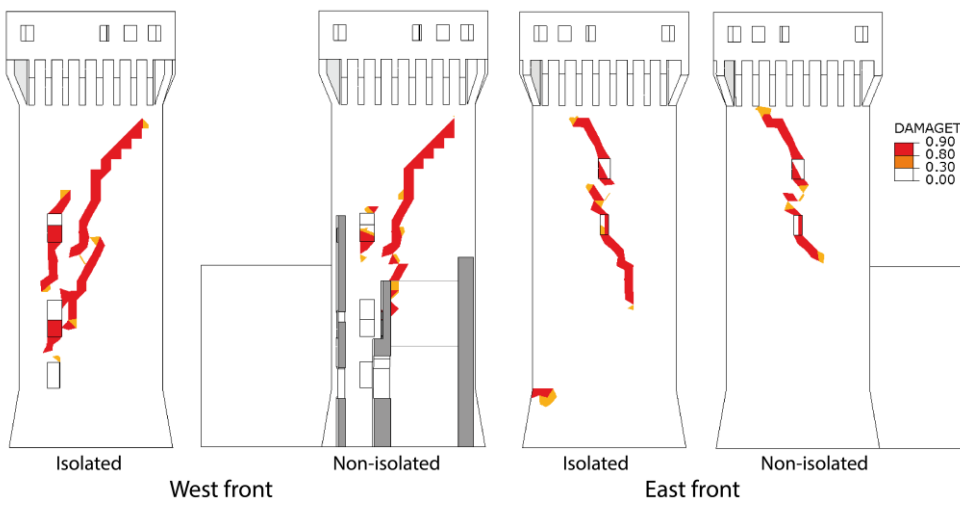Fig. 18 - Damage contour plots: West directed force (pushover analysis).

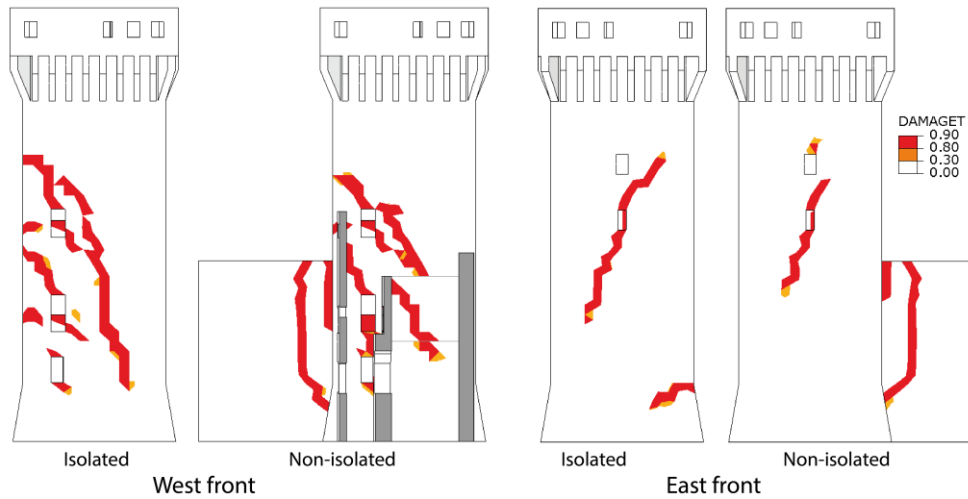Fig. 19 - Damage contour plots: North directed force (pushover analysis).

Fig. 20 - Damage contour plots: South directed force (pushover analysis).

By inspecting the pushover curves of Fig. 16 and the damage contour plots of Figs. 17-20 it appears that the greatest change between the isolated and non-isolated tower is recorded in the West load case. Therefore, for this load case a parametric study of the influence of adjacent parts' stiffness on pushover analyses has been carried out by assuming several intermediate values of δ. As expected, by decreasing the value of δ, an increment of the elastic branches' slope and of the base shear is achieved, see Fig. 21. However, also for very small values of the adjacent parts' stiffness (i.e. $\delta = 100$) it emerges a significant increment of base shear without significant changes in the elastic branch. Moreover, a considerable change of the damage pattern is obtained by decreasing the value of δ, see Fig. 22. Indeed, the main diagonal crack which extend for almost the whole height of the tower's trunk in the isolated tower ($\delta \to \infty$) tends to be confined in the upper part of the tower by decreasing the value of δ. Finally, concerning the case with $\delta = 5$ it already appears that the cracks are almost-totally confined on the upper half of the tower's trunk.
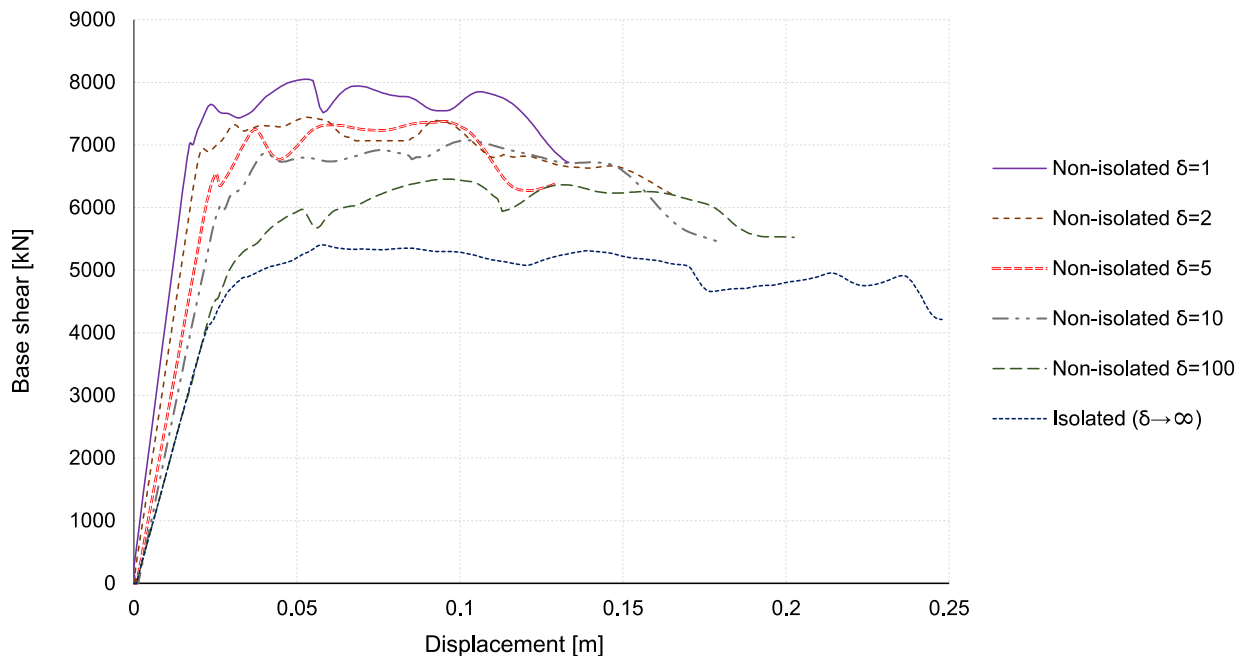

Fig. 21 - Influence of adjacent parts' stiffness on the pushover curve: West directed force.
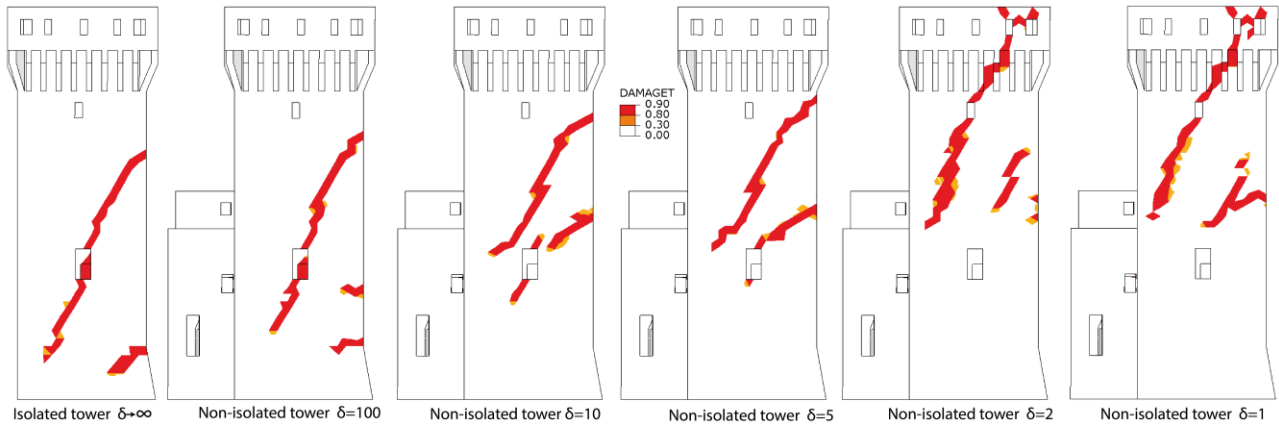
Fig. 22 - Influence of adjacent parts' stiffness on the crack pattern: West directed force (pushover analysis).

5.3 Nonlinear dynamic analyses

Here, nonlinear dynamic analyses results are presented and discussed. The suitability of both the mesh and the constitutive model for nonlinear analyses have been assessed in the previous section. Anyway, an additional aspect which characterizes dynamic simulations is the damping. Indeed, the magnitude of the structural response (displacements, velocities and accelerations) recorded in dynamic simulations are significantly influenced by the damping. The definition of reliable damping models for masonry structures is still an open problem (Elmenshawi et al. 2010). Here, a Rayleigh damping model has been used for each dynamic simulation assuming that the global damping matrix C is obtained as a linear combination of the global stiffness K and mass M matrices:

$$C = aM + bK$$

where a and b are constants of proportionality:

$$a = \frac{2\omega_1\omega_2(\xi_2\omega_1 - \xi_1\omega_2)}{\omega_1^2 - \omega_2^2}; \quad b = \frac{2(\xi_1\omega_1 - \xi_2\omega_2)}{\omega_1^2 - \omega_2^2}$$

being ξ_1 and ξ_2 two values of the damping ratio at two chosen frequencies ω_1 and ω_2. In the performed nonlinear dynamic analyses the values of a and b for the Raleigh damping model were determined by assuming for ω_1 and ω_2 the natural circular frequencies of the two principal modes and for ξ_1 and ξ_2 the values 0.05 and 0.10 respectively, as suggested for masonry structures in Peña et al. (2010) and Chiozzi et al. (2015).

As in the previous section, for the sake of brevity and in order to enhance the differences between considering an isolated tower rather than a non-isolated tower, only the nonlinear dynamic analysis results of the extreme cases of isolated tower ($\delta \rightarrow \infty$) and non-isolated tower (with $\delta = 1$) are presented.

A first dynamic simulation has been performed by applying the only EW component of the considered earthquake on both the isolated and non-isolated tower, see Fig. 23. As can be noted, the displacement time-history of the non-isolated tower shows greater maximum and residual displacements than the isolated tower, see Fig. 23a. In particular, such displacements are recorded along the East direction. In addition, by comparing the damage contour plots (Fig. 23b) arises that in the isolated tower two almost-specular diagonal cracks appear in the tower's trunk (both in the South and North fronts), whereas only one diagonal crack appears in the non-isolated tower. Therefore, the influence of the adjacent parts is evident also in nonlinear dynamic simulations.

19
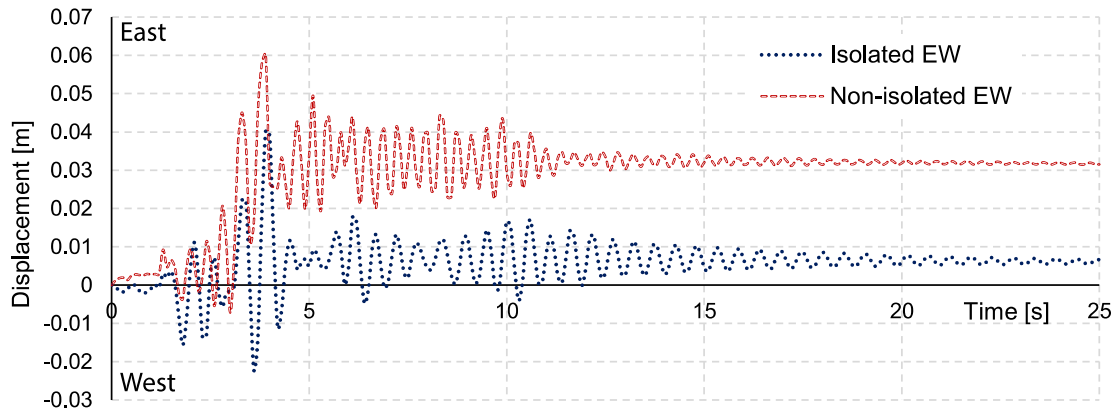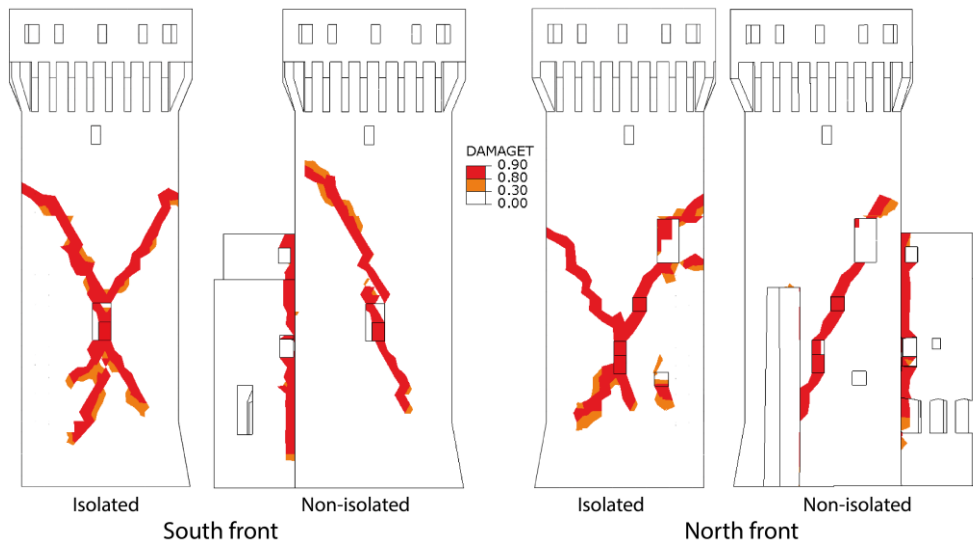
Fig. 23 - Nonlinear dynamic analyses results with the EW component of the earthquake: comparison between isolated and non-isolated tower in terms of (a) time-history and (b) damage contour plots.

Fully dynamic simulations have been carried out on the isolated and non-isolated tower accounting for the NS and EW components as well as for the NS and EW components plus the vertical component, see Figs. 24 and 25. Also in these cases, a strong influence of the adjacent parts on the seismic behavior of the tower is recorded. Indeed, maximum and residual displacements change sign from North to South and from West to East passing from the isolated to the non-isolated tower cases, see Fig. 24. Such a change is more pronounced in the EW time-history than in the NS one. In addition, the greatest residual displacement is recorded along the East direction for the non-isolated tower. Furthermore, the displacements recorded for the load case with vertical component are systematically greater than the ones without cases for both the isolated and non-isolated tower. Also, the damage contour plots at the end of such simulations (Fig. 25) shows the influence of the adjacent parts on the damage distribution. Moreover, by comparing Fig. 25a with Fig. 25b it emerges the influence of the vertical component on the damage pattern. Indeed, a slight change of the tower's trunk crack pattern is observed with, however, an increase of the damage in the tower's crowing in the case with vertical component.
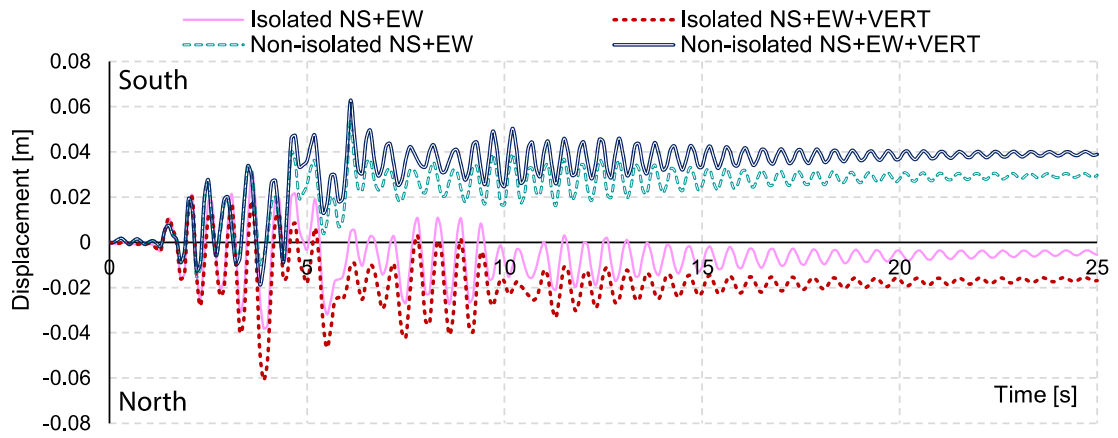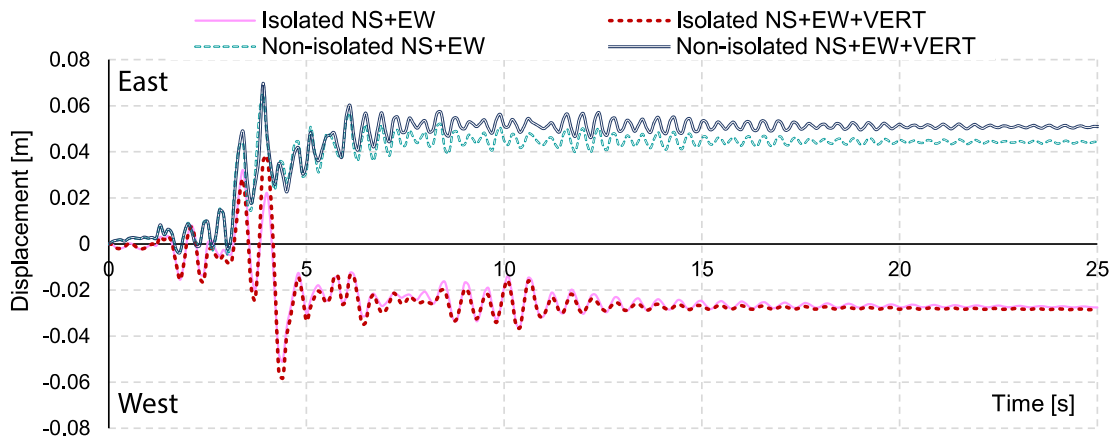
Fig. 24 - Nonlinear dynamic analyses time-history displacement: (a) NS direction and (b) EW.
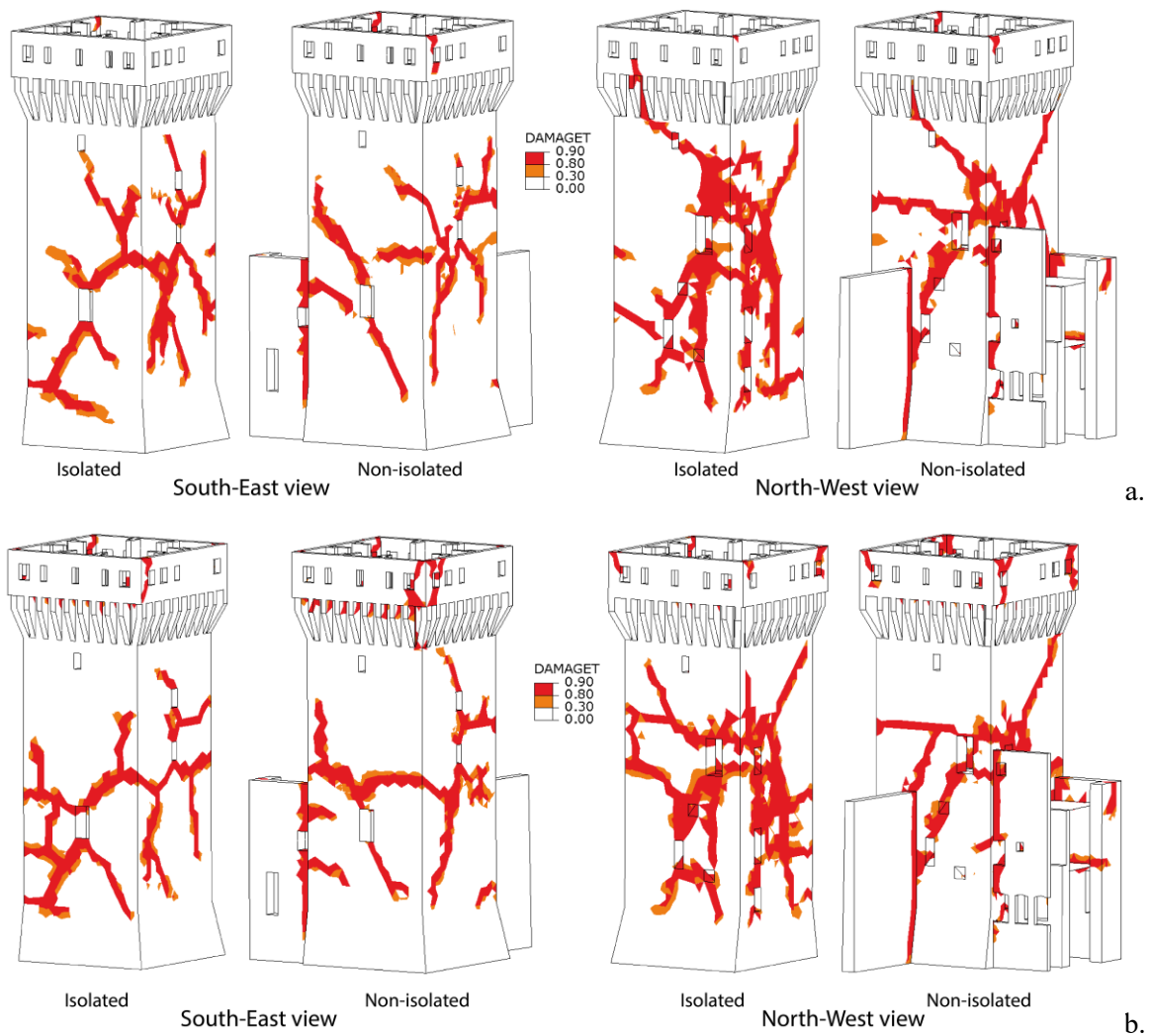
Fig. 25 - Nonlinear dynamic analyses damage contour plots: (a) without and (b) with vertical component.

6   Results comparison

The comparison between the results of nonlinear static and dynamic analyses in terms of displacements is shown in Fig. 26. In particular, the displacement demands evaluated through the pushover analyses, d_{dem}, are reported in green color, the maximum displacements recorded in the nonlinear dynamic analyses, d_{max}, are reported in red color and the residual displacements of the dynamic analyses d_{res} are reported in yellow color. The displacements of the dynamic analyses depicted in Fig. 26 are related to the case with the combined NS, EW and vertical recorded components. The seismic demand displacements of pushover analyses have been compared with the maximum displacements recorded in dynamic analyses since they are both related to the effect of an earthquake on the structure. This is further motivated as the intensity (PGA) of the accelerogram used in dynamic analyses is akin to the design action one.
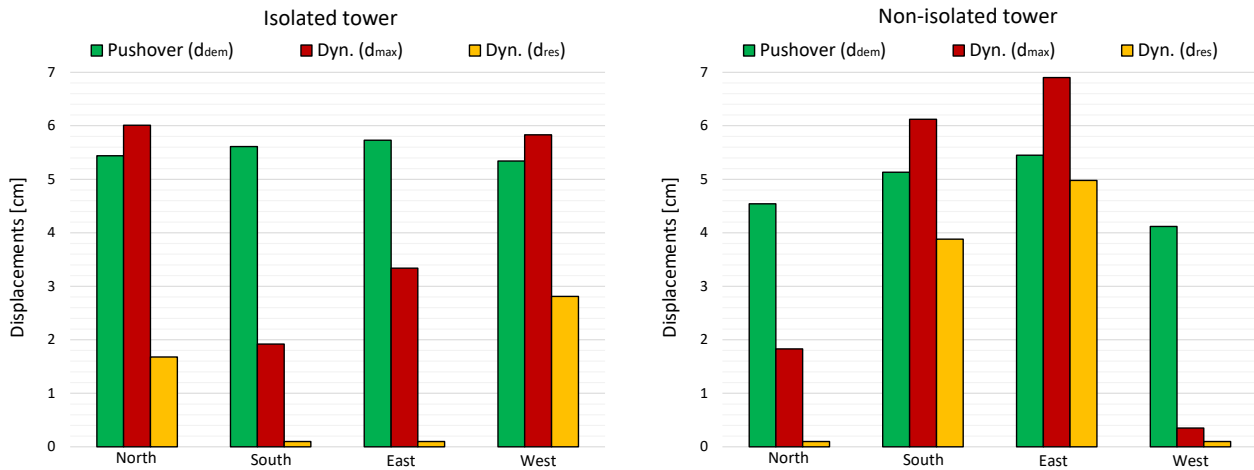
Fig. 26 - Results comparison: the displacement demand of the pushover analyses, the maximum displacement and the residual displacement of the nonlinear dynamic analyses.

Particularly, Fig. 26 shows that for pushover analyses the seismic demand displacement in East direction is slightly greater than in the others, both in the isolated and non-isolated tower. Furthermore, the displacement demands evaluated with pushover analyses are reasonably comparable to the maximum displacements evaluated with nonlinear dynamic analyses.

As regards the residual displacements of dynamic simulations, they are deeply influenced by the presence of adjacent parts. In fact, as it can be noted, the presence of adjacent portions changes the direction of residual displacements from West (isolated tower) to East (non-isolated tower) and from South to North. Generally, the results of the non-isolated tower are more in agreement with the actual behavior of the tower than those of the isolated tower. Focusing the attention on the EW direction, Fig. 27 shows a significant residual displacement of the tower in the East direction, in agreement with the numerical results of the non-isolated tower. Moreover, also the maximum displacement of the dynamic simulations is recorded in the East direction.
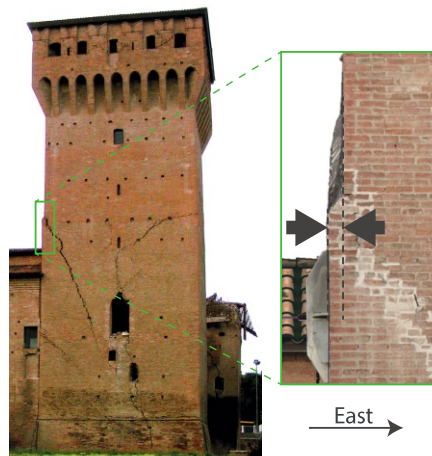

Fig. 27 - Actual residual displacement.

The actual crack pattern of the main tower is shown in Fig. 28. The main and more severe cracks are depicted through thicker lines and local collapses of masonry portions are filled with a red diagonal texture. Comparing the actual crack pattern with the numerical predictions (both nonlinear static and dynamic), several similarities appear. In particular, it arises that the main diagonal cracks (thicker lines in North and South front, Fig. 28) are captured with a reasonable accuracy by both nonlinear static analyses (Fig. 17) and nonlinear dynamic analyses (Figs. 23 and 25), especially for the simulations which consider the adjacent parts of the tower. Indeed, concerning the West load case (Fig. 22), it appears that the adjacent parts deeply influence the crack pattern. By comparing the actual crack pattern (Fig. 28, South front) with Fig. 22, it arises that the non-isolated tower

with $\delta \geq 5$ seems to better fit the actual crack pattern, since such cracks are constricted in the upper half of the tower's trunk. Furthermore, a good agreement between the damage prediction and the actual crack pattern is also observed for the West front, i.e. the side of the tower connected with the adjacent South entrance building (for instance, compare Fig. 20 with Fig. 28, West front).

The simulated crack pattern of the East front (Figs. 19 and 20) is not completely in agreement with the actual one (Fig. 28, East front), especially for what concerns dynamic simulation, see Fig. 25. In addition, the smaller cracks appeared on the tower (Fig. 28) are reproduced more coarsely. This could be addressed to the fact that small cracks are more influenced by the specific masonry texture than large cracks, and the actual masonry texture is not contemplated in the adopted homogenized model.

Finally, it has to be pointed out that, although nonlinear static and dynamic analyses of monumental buildings are usually characterized by high computational costs, the nonlinear analyses, carried out on a standard workstation (processor Intel Xeon 3.10GHz) requested a moderately short amount of time. In particular, nonlinear static analyses needed an average computational time of 4 hours and 40 minutes, whereas 25-seconds nonlinear dynamic simulations lasted for approximately 18 hours.
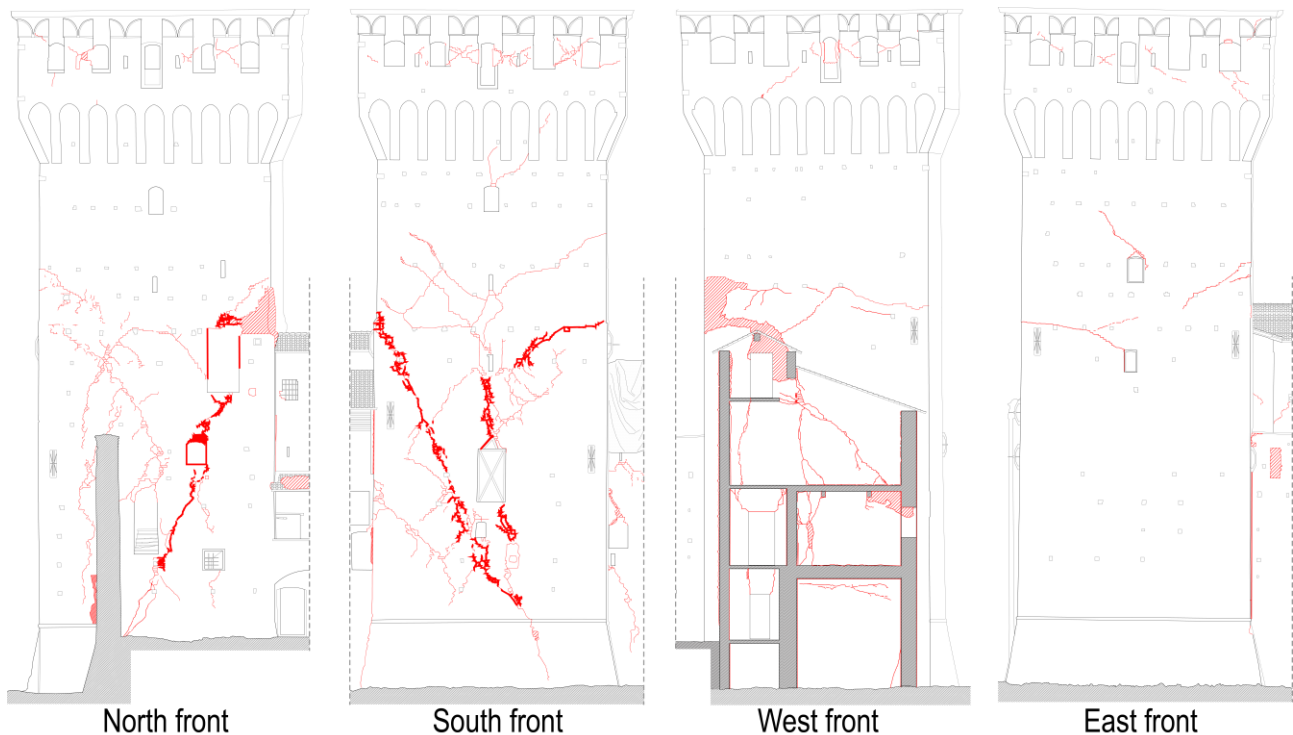

Fig. 28 - Actual crack pattern of the main tower.

7   Conclusions

In this paper, numerical insights on the seismic behavior of a non-isolated historical masonry tower have been presented and discussed. The main tower of the fortress of San Felice sul Panaro, which has been damaged by the Emilia Earthquake, has been studied.

In order to understand the behavior of the structure, its interaction with the adjacent buildings and the reasons of the occurred damage, advanced numerical analyses have been carried out on a 3D FE model with different level of constraint offered by the adjacent structural elements (from isolated to non-isolated conditions of the tower). The displacement demands evaluated with pushover analyses are reasonably comparable to the maximum displacements evaluated with nonlinear dynamic analyses. Furthermore, the results of the conducted numerical campaign shown a good agreement with the actual crack pattern, particularly for the analyses which considered the interaction with the adjacent parts of the tower. Indeed, the numerical results highlight that the crack pattern evaluated on the isolated tower is significantly different from the one evaluated on the non-

24

isolated tower, with the same load conditions. Therefore, the presence of shorter adjacent structural elements considerably changes the seismic behavior of the tower, modifying the tower's crack pattern. In the actual seismic behavior of the tower, the presence of adjacent structural elements has led the pounding between the neighboring parts. Such a phenomenon has not yet been adequately analyzed for masonry structures by the scientific community and need to be further studied. However, the role of the mono-lateral effect provided by the adjacent structural elements has been highlighted in the pushover curves, for opposite directions of the load, and in nonlinear dynamic analyses time-histories. It is worth to note that, as the studied tower represent a recurrent structure in the medieval architecture (Cattari et al. 2014), the issues discussed in the paper can be extended to similar towers with shorter adjacent structural elements.

Acknowledgements

Appendix

The displacement demand d_{dem} obtained from the transformation of the MDOF structure in an equivalent SDOF system is determined using the following standard analytical relationship (DM 14/01/2008):

$$d_{dem} = \begin{cases} \left[1 + \left(R_\mu - 1\right)\dfrac{S_{de}(T^*)}{R_\mu}\right]\Gamma, T^* < T_C \\ S_{de}(T*)\Gamma, T^* \geq T_C \end{cases}$$

where:

- $\Gamma = \dfrac{\sum m_i \Phi_i}{\sum m_i \Phi_i^2}$ is the transformation factor, where Φ_i is the i-th component of the eigenvector Φ_i and m_i is the mass of the node i;
- T_C is the corner period of the plateau of the acceleration-displacement response spectrum;
- T^* is the period of the equivalent SDOF system (the procedure for the reduction of the pushover curve to an equivalent SDOF system with a bilinear elastic-perfectly plastic force-displacement diagram is reported in detail in DM 14/01/2008;
- $S_{de}(T^*) = \dfrac{T^{*2}}{4\pi^2} S_{ae}(T^*)$ is the elastic displacement response spectrum. $S_{ae}(T^*)$ is the elastic acceleration response spectrum, where the spectral accelerations are defined as a function of the period, according to DM 14/01/2008, by assuming a seismic action with a return period of 495 years for the site of San Felice sul Panaro;
- $R_\mu = S_{ae}/S_{ay}$ is a reduction factor and it can be determined as the ratio between S_{ae} the acceleration of the SDOF system with unlimited linear behavior and S_{ay} the yield acceleration of the SDOF system with limited strength.

References

1. Abaqus®. Theory manual, version 6.14; 2014.
2. Acito, M.; Bocciarelli, M.; Chesi, C.; Milani, G. (2014) Collapse of the clock tower in Finale Emilia after the May 2012 Emilia Romagna earthquake sequence: Numerical insight. Engineering Structures, 72, 70-91.
3. Acito, M.; Chesi, C.; Milani, G.; Torri, S. (2016) Collapse analysis of the Clock and Fortified towers of Finale Emilia, Italy, after the 2012 Emilia Romagna seismic sequence: Lesson learned and reconstruction hypotheses. Construction and Building Materials, 115, 193-213.
4. Bartoli, G.; Betti, M.; Giordano, S. In situ static and dynamic investigations on the "Torre Grossa" masonry tower. Engineering Structures 2013, 52, 718-733.

5. Bartoli, G.; Betti, M.; Spinelli P.; Tordini, B. (2006) An "innovative" procedure for assessing the seismic capacity of historical tall buildings: The "Torre Grossa" masonry tower (New Delhi) in: P.B. Lourenço, P. Roca, C. Modena, S. Agrawal (Eds.), Structural Analysis of Historical Constructions, 2006.

6. Bartoli, G.; Betti, M.; Vignoli, A. (2016) A numerical study on seismic risk assessment of historic masonry towers: a case study in San Gimignano. Bulletin of Earthquake Engineering, 14(6), 1475-1518.

7. Bitelli, G.; Castellazzi, G.; D'Altri, A.M.; de Miranda, S.; Lambertini, A.; Selvaggi, I. (2016) Automated voxel model from point clouds for structural analysis of cultural heritage. ISPRS - International Archives of the Photogrammetry, Remote Sensing and Spatial Information Sciences 2016, XLI-B5, 191-197. doi:10.5194/isprs-archives-xli-b5-191-2016

8. Borri, A.; Cangi, G.; De Maria, A. (2013) Caratterizzazione meccanica delle murature (anche alla luce del recente sisma in Emilia) e interpretazione delle prove sperimentali a taglio. In Proceedings of ANIDIS Congress, Associazione Nazionale Italiana Di Ingegneria Sismica, 2013, Padua, Italy [Mechanical characterization of masonry (considering also the recent Emilia earthquake) and interpretation of shear experimental tests].

9. Carpinteri, A.; Invernizzi, S.; Lacidogna, G. (2005) In situ damage assessment and nonlinear modelling of a historical masonry tower. Engineering Structures, 27(3), 387-395.

10. Casolo, S. (1998) A three-dimensional model for vulnerability analysis of slender medieval masonry towers. Journal of Earthquake Engineering, 2(4), 487-512.

11. Casolo, S.; Milani, G.; Uva, G.; Alessandri, C. (2013) Comparative seismic vulnerability analysis on ten masonry towers in the coastal Po Valley in Italy. Engineering Structures, 49, 465-490.

12. Casolo, S. (2017) A numerical study on the cumulative out-of-plane damage to church masonry façades due to a sequence of strong ground motions. Earthquake Engineering & Structural Dynamics. doi:10.1002/eqe.2927

13. Castellazzi G.; D'Altri, A.M.; Bitelli, G.; Selvaggi, I.; Lambertini, A. (2015) From Laser Scanning to Finite Element Analysis of Complex Buildings by Using a Semi-Automatic Procedure. Sensors, 15, 18360-18380. doi:10.3390/s150818360

14. Castellazzi, G.; D'Altri, A. M.; de Miranda, S.; Ubertini, F. (2017) An innovative numerical modeling strategy for the structural analysis of historical monumental buildings. Engineering Structures, 132, 229-248. doi:10.1016/j.engstruct.2016.11.032

15. Castellazzi, G.; D'Altri, A.M.; de Miranda, S.; Magagnini, S.; Tralli, A. (2016a) On the seismic behavior of the main tower of San Felice sul Panaro (Italy) fortress. AIP Conference Proceedings 2016, 1790(1), 130009. doi: 10.1063/1.4968727

16. Castellazzi, G.; D'Altri, A.M.; de Miranda, S.; Ubertini, F.; Bitelli, G.; Lambertini, A.; Selvaggi, I.; Tralli, A. (2016b) A mesh generation method for historical monumental buildings: an innovative approach. ECCOMAS Congress 2016 - Proceedings of the 7th European Congress on Computational Methods in Applied Sciences and Engineering, 2016, 1, 409-416

17. Cattari, S.; Degli Abbati, S.; Ferretti, D.; Lagomarsino, S.; Ottonelli, D.; Tralli, A. (2014) Damage assessment of fortresses after the 2012 Emilia earthquake (Italy). Bulletin of Earthquake Engineering, 12, 2333-2365.

18. Cattari, S.; Lagomarsino, S.; Resemini, S. (2012) Il ruolo delle volte nella risposta sismica degli edifici in muratura. In Archi e volte in zona sismica - Meccanica delle strutture voltate; Borri, A., Bussi, L., Eds.; Doppiavoce: Naples, Italy, 2012 [The role of vaults in the seismic response of masonry buildings].

19. Chiozzi, A.; Simoni, M.; Tralli, A. (2015) Base isolation of heavy non-structural monolithic objects at the top of a masonry monumental construction. Materials and Structures, 49(6), 2113-2130.

20. Circolare 617-02/02/2009. Istruzioni per l'applicazione delle nuove norme tecniche per le costruzioni di cui al decreto ministeriale 14 Gennaio 2008 [Instructions for the application of the new technical norms on constructions].

21. D'Altri, A.M.; Castellazzi, G.; de Miranda, S.; Tralli, A. (2017) Seismic-induced damage in historical masonry vaults: A case-study in the 2012 Emilia earthquake-stricken area, Journal of Building Engineering, 13, 224-243. http://dx.doi.org/10.1016/j.jobe.2017.08.005

22. D'Ambrisi, A.; Mariani, V.; Mezzi, M. (2012) Seismic assessment of a historical masonry tower with nonlinear static and dynamic analyses tuned on ambient vibration tests. Engineering Structures, 36, 210-219.

23. DIANA finite element analysis, release 9.5. User's manual. TNO DIANA® BV: Delft; 2013.

24. DM 14/01/2008. Nuove norme tecniche per le costruzioni. Ministero delle Infrastrutture (GU n.29 04/02/2008), Rome, Italy [New technical norms on constructions].

25. Dolce, M.; Nicoletti, N.; Ammirati, A.; Bianconi, R.; Filippi, L.; Gorini, A.; Marcucci, S.; Palma, F.; Zambonelli, E.; Lavecchia, G.; de Nardis, R.; Brozzetti, F.; Boncio, P.; Cirillo, D.; Romano, A.; Costa, G.; Gallo, A.; Tiberi, L.; Zoppè, G.; Suhadolc, P.; Ponziani, F.; Formica, A. (2012a) The Emilia thrust earthquake of 20 May 2012 (Northern Italy): strong motion and geological observations-report I, 2012. www.protezionecivile.gov.it/resources/cms/documents/Report_DPC_1_Emilia_EQSd.pdf

26. Dolce, M.; Nicoletti, N.; Ammirati, A.; Bianconi, R.; Filippi, L.; Gorini, A.; Marcucci, S.; Palma, F.; Zambonelli, E.; Lavecchia, G.; de Nardis, R.; Brozzetti, F.; Boncio, P.; Cirillo, D.; Romano, A.; Costa, G.; Gallo, A.; Tiberi, L.; Zoppè, G.; Suhadolc, P.; Ponziani, F.; Formica, A. (2012b) The Ferrara arc thrust earthquakes of May-June 2012 (Northern Italy): strong-motion and geological observations-report II, 2012 www.protezionecivile.gov.it/resources/cms/documents/report_DPC_2_Emilia_EQSBis.pdf

27. DPCM 9/2/2011. Linee guida per la valutazione e la riduzione del rischio sismico del patrimonio culturale con riferimento alle Norme tecniche delle costruzioni di cui al decreto del Ministero delle Infrastrutture e dei trasporti del 14 gennaio 2008 [Italian guidelines for the evaluation and reduction of the seismic risk of cultural heritage, with reference to the Italian norm of constructions].

28. Elmenshawi, A.; Sorour, M.; Mufti, A.; Jaeger, L. G.; Shrive, N. (2010) Damping mechanisms and damping ratios in vibrating unreinforced stone masonry. Engineering Structures, 32(10), 3269-3278.

29. Lagomarsino, S.; Cattari, S. (2015) PERPETUATE guidelines for seismic performance-based assessment of cultural heritage masonry structures. Bulletin of Earthquake Engineering, 13(1), 13-47.

30. Luciano, R.; Sacco, E. (1997) Homogenization technique and damage model for old masonry material. International Journal of Solids and Structures, 34(24), 3191-3208.

31. Luzi, L.; Hailemikael, S.; Bindi, D.; Pacor, F.; Mele, F. (2008) ITACA (ITalian ACcelerometric Archive): A web portal for the dissemination of Italian strong motion data, Seismological Research Letters, 79, 716-722.

32. Macchi, G.; Ruggeri, M.; Eusebio, M.; Moncecchi, M. (1993) Structural assessment of the leaning tower of Pisa. In Proceedings of Structural preservation of the architectural heritage, IABSE 1993, Zurich, Switzerland, pp 401-408.

33. Mazzotti, C.; Bellini, A.; Ferretti, F.; Incerti, A.; Vinciguerra, A. (2016) Prove di caratterizzazione meccanica di murature ed elementi in c.a. della Rocca Estense di San Felice sul Panaro (MO), technical report, CIRI Edilizia e costruzioni, University of Bologna, Italy, 2016 [Experimental tests for the mechanical characterization of masonries and RC elements of the fortress of San Felice sul Panaro (MO)].

34. Milani, G.; Casolo, S.; Naliato, A.; Tralli, A. (2012) Seismic Assessment of a Medieval Masonry Tower in Northern Italy by Limit, Nonlinear Static, and Full Dynamic Analyses. International Journal of Architectural Heritage, 6(5), 489-524.

35. Milani, G.; Lourenço, P.; Tralli, A. (2007) 3D homogenized limit analysis of masonry buildings under horizontal loads. Engineering Structures, 29(11), 3134-3148.

36. Mistler, M.; Anthoine, A.; Butenweg, C. (2007) In-plane and out-of-plane homogenisation of masonry. Computers & Structures, 85(17-18), 1321-1330.

37. Page, A.W. (1981) The biaxial compressive strength of brick masonry. In Proceeding of the Institution of Civil Engineers 1981, Part 2, 71, 893-906.

38. Peña, F.; Lourenço, P. B.; Mendes, N.; Oliveira, D.V. (2010) Numerical models for the seismic assessment of an old masonry tower. Engineering Structures, 32(5), 1466-78.

39. Pieraccini, M.; Dei, D.; Betti, M.; Bartoli, G.; Tucci, G.; Guardini, N. (2014) Dynamic identification of historic masonry towers through an expeditious and no-contact approach: Application to the "Torre del Mangia" in Siena (Italy). Journal of Cultural Heritage, 15(3), 275-282.

40. Pineda, P. (2016) Collapse and upgrading mechanisms associated to the structural materials of a deteriorated masonry tower. Nonlinear assessment under different damage and loading levels. Engineering Failure Analysis, 63, 72-93.

41. Preciado, A. (2015) Seismic vulnerability and failure modes simulation of ancient masonry towers by validated virtual finite element models. Engineering Failure Analysis, 57, 72-87.

42. Sarhosis, V.; Fabbrocino, F.; Formisano, A.; Milani, G. (2017) Seismic vulnerability of different in geometry historic masonry towers. In: 6th International Conference on Computational Methods in Structural Dynamics and Earthquake Engineering (COMPDYN 2017) Rhodes Island, Greece.
43. Tiberti, S.; Acito, M.; Milani, G. (2016) Comprehensive FE numerical insight into Finale Emilia Castle behavior under 2012 Emilia Romagna seismic sequence: Damage causes and seismic vulnerability mitigation hypothesis. Engineering Structures, 117, 397-421.
44. Valente, M.; Milani, G. (2016a) Seismic assessment of historical masonry towers by means of simplified approaches and standard FEM. Construction and Building Materials 2016, 108, 74-104.
45. Valente, M.; Milani, G. (2016b) Non-linear dynamic and static analyses on eight historical masonry towers in the North-East of Italy. Engineering Structures 2016, 114, 241-270.
46. Valente, M.; Milani, G. (2017). Effects of Geometrical Features on the Seismic Response of Historical Masonry Towers. Journal of Earthquake Engineering, 1-33. doi:10.1080/13632469.2016.1277438